

Physical Phenomenology of Phyllotaxis

Takuya Okabe

Faculty of Engineering, Shizuoka University, 3-5-1 Johoku, Hamamatsu 432-8561, Japan

Abstract

We propose an evolutionary mechanism of phyllotaxis, regular arrangement of leaves on a plant stem. It is shown that the phyllotactic pattern with the Fibonacci sequence has a selective advantage, for it involves the least number of phyllotactic transitions during plant growth.

Keywords: Schimper-Braun; Fibonacci number; Stern-Brocot tree; natural selection

1. Introduction

Phyllotaxis, regular arrangement of leaves on a plant stem, has since long attracted the minds of botanists, mathematicians and physicists ([24, 11, 2, 12]). Most commonly, alternate leaves along a twig execute a spiral with an angle of $1/2$, $1/3$, $2/5$, $3/8$ of a full rotation, or otherwise with a limit angle of 137.5 degrees (Fig. 1). Patterns with the other fractions are also observed, though uncommonly. Hence phyllotaxis is regarded not as a universal *law* but as a fascinatingly prevalent *tendency* ([4]). For decades, mathematical works have elucidated number theoretical structure of phyllotaxis and deepened our understanding of the subject significantly ([5, 1, 17, 15, 18, 19, 20, 14]). Nevertheless, there still remains a fundamental problem of why and how only some specific numbers are favored by nature. This is a problem of natural science.

Physical or chemical models studied thus far are mostly based on *dynamical* mechanism, according to which a phyllotactic pattern is supposed to be realized autonomously as an end result of its own mechanical or chemical dynamics ([1, 25, 20, 14, 6]). This is mechanical determinism. Mathematicians and physicists generally appreciate this point of view. On the contrary, biologists generally take the opposite viewpoint that there are so strong reasons for the plants to have genetic information that a divergence angle between adjacent leaves must be determined genetically. This is genetic determinism. In this case, we still have to make clear how the plants inherit the mathematical characteristics, i.e., a *static* or statistic mechanism of phyllotaxis is asked for. When it comes down to it, there seems no hope to do without mathematics, for we have to explain why the divergence angle is programmed to take neither 130° nor 140° but the magic number 137.5° . Unfortunately, candidate explanations have been only descriptive and qualitative, or otherwise quantitative but *teleological* such that packing efficiency ([17]) or uniformity ([15, 18, 3]) is meant to be maximized resultingly. In any case, at this fundamental level, we have to regard

phyllotaxis as a conundrum of theoretical physics (or theoretical biology), for we have to deal with mathematics observed in the real world. The aim of this paper is to present a satisfactory static mechanism to be contrasted not only with the existing dynamical models but with the teleological explanations.

We propose a new mechanism based on a growth model of a plant. The model is basically characterized by two parameters, an initial (preset) value of the divergence angle, $2\pi\alpha_0$, and a vertical range of repulsive interaction, n_c . The model is based on the observation that a plant has inherent abilities (1) to arrange leaves primarily on a regular spiral with a constant angle of rotation $2\pi\alpha_0$, and (2) to exert secondary torsions between the leaves within reach of n_c . The former is consistent with experiments on apical meristems ([8, 23]). The latter is supposed to operate in a vascular system ([13]). The secondary interaction reinforces the regularity of the helical arrangement, thereby the observed angle α generally undergoes changes from the initial value α_0 . With the vertical range n_c regarded as a growth index, it is shown that α goes through stepwise transitions between phyllotactic fractions (PF) in the course of the growth (Fig. 6). In fact, many plants progress through distinct phyllotactic transition (PT) during early stages of development. It should be rather remarked that the secondary changes, essential for us, are usually noticed but often disregarded as irrelevant (as secondary). To outline the proposed mechanism, consider a population of random samples with all possible values of the preset angle α_0 , and let them grow according to the model. As they grow, each sample will exhibit its own PTs respectively, depending on α_0 . With all the grown samples, we leave from formal analysis. At this point, we appeal to biological reasoning according to natural selection, by which all but that with the golden angle $2\pi\alpha_0 = 137.5^\circ$ turns out to be eliminated. The selected sample is favored in nature, for it is structurally the most stable because it undergoes the least PTs. To put it concretely, we show how the num-

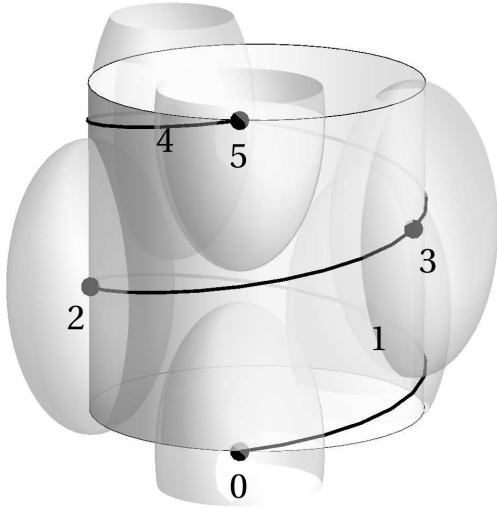


Figure 1: A pattern with a phyllotactic fraction (PF) $\alpha = 2/5$. The angle between consecutive leaves (points) is $2/5$ of a rotation. As a guide to the eye, a spiral, called the ontogenetic or genetic spiral, is drawn through the points in their order of succession. Repulsive interaction between the points is represented by (imaginary) prolate spheroids around the points.

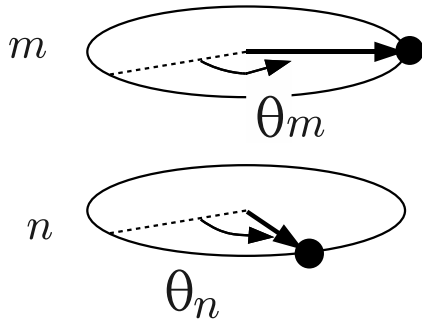


Figure 2: Interaction $V_n(\theta_m - \theta_n, m - n)$ between the points (m, θ_m) and (n, θ_n) is periodic in $\theta_m - \theta_n$ with a period of 2π . By definition of X and n_c , $V_n(\theta_m - \theta_n, m - n)$ vanishes for $X < |\theta_m - \theta_n|/2\pi < 1$ and $|m - n| > n_c$.

ber of PTs, N_{PT} , depends on the preset angle α_0 and the growth index n_c (Fig. 8). To the author's knowledge, no such mathematical *evolutionary* mechanism of phyllotaxis has ever been put forward.

2. Model

We restrict ourselves to the most common case of a spiral or helical pattern with a single 'leaf' at each level (node). We use an integer n to label successive points along a genetic spiral (Fig. 1), whose positions are given by the coordinates (θ_n, n) or by (x_n, n) in terms of $\theta_n = 2\pi x_n$. In this dimensionless representation with normalized length scales, the coordinate may be regarded to represent the position of either leaf primordia on apical meristem or leaf traces in vascular system. Here the important

point is that physical quantities are periodic with respect to the angular coordinate θ_n . The angle θ_n is measured from $\theta_0 = 0$ for $n = 0$, and is regarded to take a value within $-\pi \leq \theta_n < \pi$ (or $-1/2 \leq x_n < 1/2$). To describe phenomenologically a torsional force between two points (θ_n, n) and (θ_m, m) ($n \neq m$), we introduce repulsive interaction $V_n(\theta_m - \theta_n, m - n)$ (Fig. 2). As a theoretical and phenomenological tool to clarify number theoretical structure of the macroscopic phenomenon, details for implementation of the interaction need not be specified.

For the sake of simplicity and convenience, let us write

$$V_n(2\pi x, m) = u_n V(2\pi x, m) = u_n v_m V(x). \quad (1)$$

The angular dependence is represented by $V(x)$ and the vertical (internode) dependence is described with v_m , both of which are defined by the last equation. The factor u_n represents the dependence on the subscript n of $V_n(2\pi x, m)$, which occurs because translational invariance along the stem (in the vertical direction) is broken in general. However, it turns out that the factor u_n drops out of our problem.

The interaction $V_n(\theta, m)$ is characterized by two parameters. They are finite ranges of $V_n(\theta, m)$, in the angular direction θ (or $x = \theta/(2\pi)$), and in the vertical direction m . For the former, we introduce a half-width $X (< 1/2)$ of $V(x)$, i.e.,

$$\begin{aligned} V(x) &> 0, & 0 \leq |x| < X, \\ V(x) &\simeq 0, & X < |x| < 1/2. \end{aligned}$$

For example, let us use

$$V(x) = e^{-(\frac{2\pi}{X})^2}, \quad |x| \leq 1/2. \quad (2)$$

Note that $V(x)$ is periodic so that $V(x) = V(x + 1)$, and we may set $V(0) = 1$ arbitrarily. In terms of the width X thus defined, the angular width of the original interaction $V_n(\theta, m)$ is given by

$$\Delta\theta \simeq 4\pi X. \quad (3)$$

The second parameter is the vertical range of influence n_c . By definition, we have $V_n(\theta, m) > 0$ for $0 < m \leq n_c$ and $V_n(\theta, m) \simeq 0$ for $m > n_c$, or

$$\begin{aligned} v_n &> 0, & 0 < n \leq n_c, \\ v_n &\simeq 0, & n_c < n. \end{aligned}$$

In what follows, n_c plays an important role.

We investigate a regular spiral arrangement with the *divergence angle* $2\pi\alpha$, namely,

$$\theta_n = 2\pi n\alpha. \quad (x_n = n\alpha.) \quad (4)$$

In principle, the phyllotactic index α may take any real number (Fig. 1). Nevertheless, in our model, and in real life, α turns out to be a fraction, called *phyllotactic fraction* (PF). Phenomenologically, α obeys a mechanical relaxation equation,

$$\frac{d\alpha}{dt} = -\frac{dE}{d\alpha}. \quad (5)$$

The right-hand side is a torsional force, represented by the total interaction E ,

$$E = \sum_{n=0}^{\infty} \sum_{m>n} V_n(\theta_m - \theta_n, m - n) \quad (6)$$

$$= \sum_{n=0}^{\infty} \sum_{m=1}^{\infty} V_n(2\pi m\alpha, m). \quad (7)$$

Substituting Eq. (1), we obtain

$$E = v(\alpha) \sum_{n=0}^{\infty} u_n, \quad (8)$$

where

$$v(\alpha) = \sum_{m=1}^{\infty} v_m V(m\alpha). \quad (9)$$

The factor $\sum_{n=0}^{\infty} u_n$ in Eq. (8) may be dropped hereafter, as it is a constant independent of α . Substituting Eq. (8) in Eq. (5), we find the phyllotactic index α in static equilibrium as a minimum of the effective interaction $v(\alpha)$. For instance, when $v(\alpha)$ has a single minimum at $\bar{\alpha}$, we may assume a parabolic potential $E = \frac{k}{2}(\alpha - \bar{\alpha})^2$ around the minimum $\alpha \simeq \bar{\alpha}$. Then we obtain $\frac{d\alpha}{dt} = -k(\alpha - \bar{\alpha})$ from Eq. (5), and $\alpha(t) = \bar{\alpha} + (\alpha(0) - \bar{\alpha})e^{-kt}$ as a solution. Therefore, in the end, we reach static equilibrium at the minimum $\alpha(\infty) = \bar{\alpha}$, irrespective of the initial value $\alpha(0)$. In general, $v(\alpha)$ may have many local minima. To which minimum α evolves into depends on the initial value $\alpha(0)$. This is the third parameter α_0 ,

$$\alpha(0) = \alpha_0. \quad (10)$$

We introduced several quantities to define our model. Among others, n_c and α_0 are the most important. Main results given below are not affected essentially by the other quantities as X and v_m for $v(\alpha)$ in Eq. (9). In the next section, we investigate conditions to realize a local minimum of $v(\alpha)$. Hereafter we restrict ourselves to $0 < \alpha \leq 1/2$, because $v(1 - \alpha) = v(-\alpha) = v(\alpha)$ by bilateral symmetry.

3. Results

3.1. Phyllotactic Fraction (PF)

By way of illustration, $v(\alpha)$ in Eq. (9) is plotted for $n_c = 5, 6$ and 7 in Fig. 3, where we use Eq. (2) with $X = 0.1$ and $v_n = 0.8^n$ for $n \leq n_c$.

Consider the case $n_c = 5$, the solid curve in Fig. 3. We observe that $v(\alpha)$ has five minima. In effect, they lie around fractions $\alpha = 1/6, 2/9, 2/7, 3/8$ and $3/7$. Let us increase n_c from 5 to 7 to see if the minima are affected. For $n_c = 7$, the two minima at $2/9$ and $3/8$ remain almost intact, whereas the other three minima $1/6, 2/7$ and $3/7$ for $n_c = 5$ are lost (Fig. 3).

To reach the minimum at PF $3/8$, the initial value α_0 has to be in a range $1/3 \lesssim \alpha_0 \lesssim 2/5$. Let us introduce

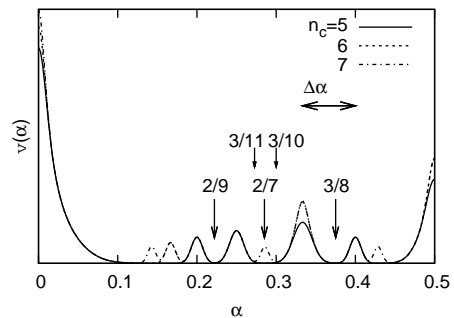


Figure 3: Effective interaction $v(\alpha)$ for $n_c = 5, 6$ and 7 ($X = 0.1$ and $v_n = 0.8^n$ for $n \leq n_c$). To reach a minimum at $\alpha = 3/8$, the initial value α_0 must fall within $\Delta\alpha$ denoted by the double-headed arrow.

the total width $\Delta\alpha$ of a range allowed for α_0 . For PF $3/8$, we have $\Delta\alpha = \frac{2}{5} - \frac{1}{3} \simeq 0.067$. The range is indicated with the double-headed arrow in Fig. 3. Similarly, we get $\Delta\alpha \simeq 0.05$ for $2/9$, which is narrower than $\Delta\alpha \simeq 0.067$ for $3/8$. Therefore, if α_0 is to be chosen randomly for a fixed n_c , it would be $(0.067/0.05=1.3)$ times easier to realize PF $3/8$ than to realize $2/9$.

From Fig. 3, we note that the minimum at $2/7$ for $n_c = 5$ and 6 turns into a local *maximum* for $n_c = 7$. Similarly, the minimum at $\alpha = 3/8$ becomes a maximum for $n_c = 8$ (not shown in Fig. 3), whereas the minimum at $2/9$ remains intact for $n_c = 5, 6, 7$ and 8 . For each PF, we define n_0 and Δn by the condition

$$n_0 \leq n_c \leq n_0 + \Delta n \quad (11)$$

for the fraction to be a minimum. We obtain $(n_0, \Delta n) = (5, 2)$ for $3/8$, and $(n_0, \Delta n) = (5, 3)$ for $2/9$.

When a minimum becomes a maximum, two new minima appear on both sides of the maximum. For example, the local minimum at $\alpha = 2/7$ for $n_c = 5, 6$ ($(n_0, \Delta n) = (4, 2)$) becomes a local maximum at $n_c = 7$. When a ‘mother’ PF $2/7$ is lost to become the maximum, it is flanked on both sides by two newborn ‘daughter’ minima at $3/11$ and $3/10$ (Fig. 3). In other words, the mother PF $\alpha = 2/7$ branches (fissions) into the daughter PFs $3/11$ and $3/10$ at $n_c = 7$.

In this manner, we can locate the positions of the local minima of $v(\alpha)$ and construct their branching structure. They are shown in Fig. 4, where each dot representing a minimum is labeled with a fraction (PF). In Fig. 4, there is a vertical segment stretching upward from each dot. The length of the segment is Δn for the fraction. In Fig. 5, we plot the fractions in the Δn - $\Delta\alpha$ plane, as well as in the Δn - $\Delta\alpha$ - n_0 space. In the figures, the observed main sequence of phyllotaxis is drawn with the bold line.

In the above and the following, we make good use of the interesting and important property of the model that the divergence angle α of a phyllotactic pattern is given by a fraction (PF). Indeed, deviation from an exact fraction may be expected in general. This is discussed in Sec. 4.

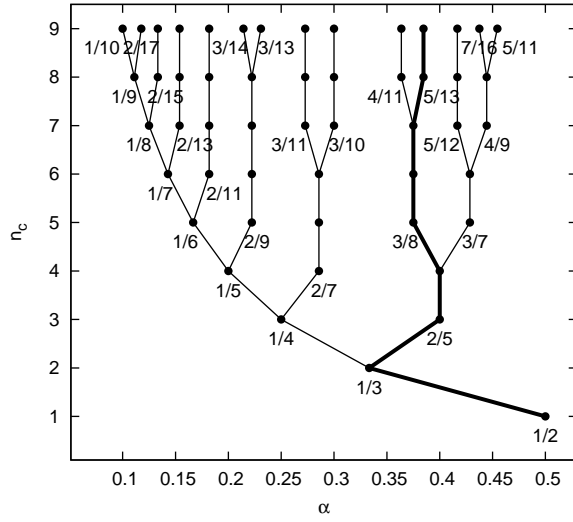


Figure 4: Position α of a local minimum of $v(\alpha)$ is represented by a point labeled with a fraction. Lines connecting the points represent hierarchical branching structure of the fractions. The length of the vertical segment stretching from a point represents Δn for the fraction (e.g., $\Delta n = 0$ for $1/4$ and $\Delta n = 1$ for $2/5$). Fractions on the bold line comprise the main sequence of phyllotaxis.

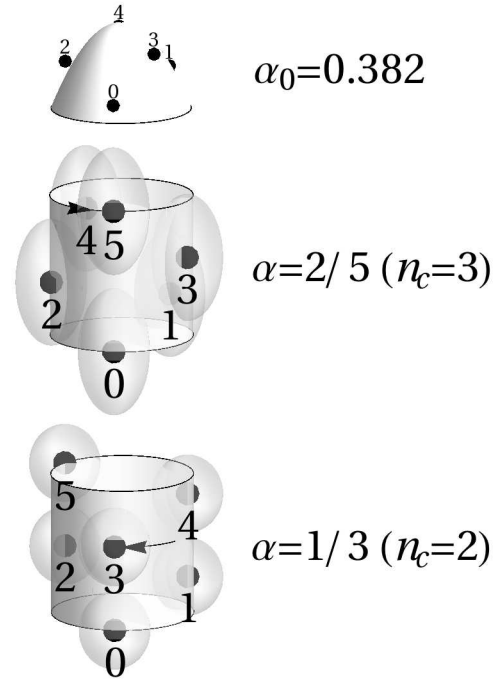


Figure 6: An initial pattern ($\alpha_0 = 0.382$) of leaf primordia on the apex (top). A ‘developing’ leaf pattern for $\alpha = 2/5$ ($n_c = 3$) (middle) lies on top of a ‘mature’ leaf pattern for $\alpha = 1/3$ ($n_c = 2$) (bottom). Torsional motion is indicated by an arrow.

3.2. Phyllotactic Transition (PT)

To compare with a real plant, we regard n_c as a growth index. This is reasonable because the increase of n_c in our normalized (cylinder) representation corresponds to a decrease of plastochron ratio in a disc representation ([16]), and to a decrease of the internode distance if it were introduced explicitly ([1]). The index n_c , presumably related to the length of leaf-trace primordia, is supposed to increase in the course of plant growth so that a stem is vertically organized into zones with different values of n_c . In a developing leaf zone near the apex, n_c is large. In a mature leaf zone near the plant base, n_c is small. For a given value of α_0 , we obtain patterns for different n_c standing in a row along the stem, as illustrated in Fig. 6. Thus we explain *phyllotactic transition* (PT), the transition of α between different PFs along the stem.

For given n_c , from Fig. 4 we can read α resulting from arbitrary α_0 . Firstly, locate the reference point (α_0, n_c) in the figure. Then, the PF α is selected from the neighboring two minima on both sides of the reference point by comparing the horizontal coordinate α_0 with that of a maximum between the two minima. If α_0 is on the left (right) of the maximum, then the minimum in the left (right) hand side is chosen. For example, for $\alpha_0 \simeq 0.3$, we get $\alpha = 1/2$ for $n_c = 1$, and $\alpha = 1/3$ for $n_c = 2$. For $n_c = 3$, we choose $\alpha = 1/4$ from the two minima $1/4$ and $2/5$ because $\alpha_0 \simeq 0.3 < 1/3$, the maximum between the

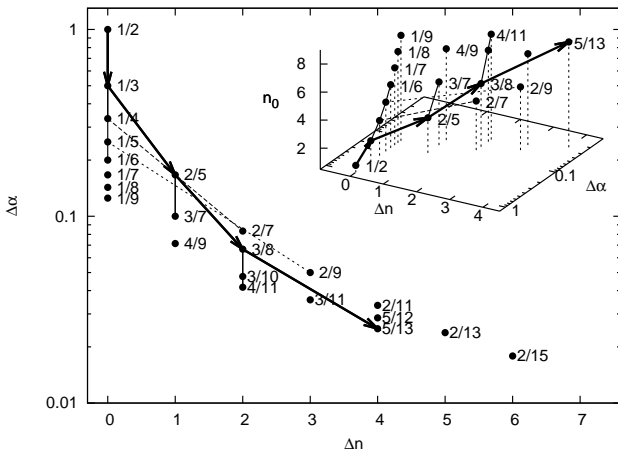


Figure 5: For lower order fractions in Fig. 4, $\Delta\alpha$ is plotted against Δn . The inset shows a 3D plot of n_0 against Δn and $\Delta\alpha$ (defined in Sec. 3.1). The bold arrows represent the main sequence.

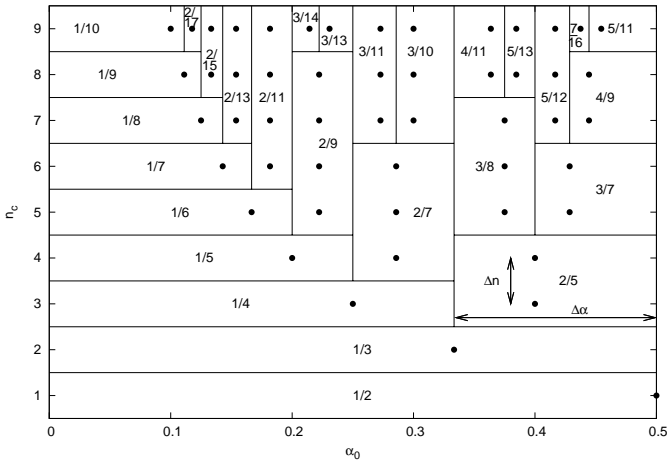


Figure 7: Diagram for phyllotactic fractions (PF). PF $\alpha = 2/5$ is obtained for $n_c = 3, 4$ and $1/3 < \alpha_0 < 1/2$ ($\Delta n = 1, \Delta\alpha = 0.17$).

two minima.

As a result, we obtain a diagram in Fig. 7. The diagram may serve to get PF α for arbitrary pair (α_0, n_c) . In Table 1, sequences of PF α for randomly chosen values of α_0 are given representatively. With real plants in mind, four of them are displayed in Fig. 8.

3.3. Mechanism of Phyllotaxis

Nature's preference of particular PFs is accounted for simply by the following hypothesis: (H) *A phyllotactic pattern of a fraction with larger Δn is more favored.*

For $n_c = 3$ in Fig. 4, we have two possible patterns $\alpha = 1/4$ or $2/5$, depending on α_0 . According to (H), the latter $2/5$ is favored, because $\Delta n = 1$ for $2/5$ is larger than $\Delta n = 0$ for $1/4$. In this manner, as n_c is increased, the hypothesis (H) gives us a sequence on the thick line in Figs. 4 and 5, that is,

$$1/2, 1/3, 2/5, 3/8, 5/13, \dots \quad (12)$$

This is the *main sequence* of phyllotaxis almost always observed. In fact, the main sequence covers more than 90% of all observed cases ([11]). The numerator and the denominator of the PF in (12) are alternate numbers of a Fibonacci sequence,

$$1, 1, 2, 3, 5, 8, 13, 21, 34, 55, 89, 144, \dots, \quad (13)$$

in which every number is the sum of the preceding two. As a limit number of the sequence in (12), we obtain $\alpha = (3 - \sqrt{5})/2 \simeq 0.381966$ ($2\pi\alpha \simeq 137.5^\circ$), the golden angle or the Fibonacci angle.

We argue that the hypothesis (H) is biologically plausible, because the larger Δn ensures the more stability against expected variations of the growth index n_c . To show this explicitly, let us define N_{PT} as the number of PTs encountered in a sequence for a given α_0 . N_{PT} counts

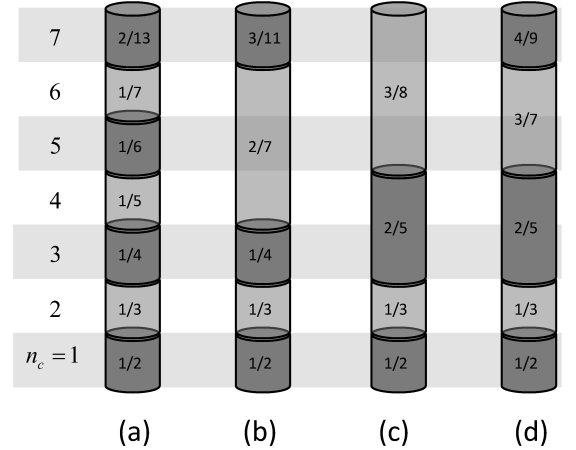


Figure 8: Lower part of four sequences in Table 1 are displayed vertically. (a) $\alpha_0 = 0.146317$ ($N_{PT} = 6$), (b) $\alpha_0 = 0.281978$ ($N_{PT} = 4$), (c) $\alpha_0 = 0.375791$ ($N_{PT} = 3$), (d) $\alpha_0 = 0.469168$ ($N_{PT} = 4$). The most favorable is (c) with the least number of phyllotactic transitions ($N_{PT} = 3$).

how many times PF α changes as the index n_c is increased, so that it depends on α_0 and the upper bound of n_c . Hence N_{PT} may be used as a measure of stability of a pattern with a given phyllotactic sequence. By definition, N_{PT} is small for a sequence comprised of PFs with small Δn . Therefore, (H) may be rephrased as follows: (H') *A favorable sequence has small N_{PT} .*

Biological implications of (H') may be understood intuitively from Fig. 8. According to (H'), the case (c) for $\alpha_0 \simeq 0.38$ ($2\pi\alpha_0 = 137.5^\circ$) is the most favorable, because $N_{PT} = 3$ for (c) is the smallest of all. What this means must be quite obvious from the figure. We give N_{PT} in the last column of Table 1. See the eighth row for $\alpha_0 = 0.375791$ in Table 1. We find that N_{PT} is the smallest for the main sequence, (12), for $\alpha_0 \simeq 0.38$ ($2\pi\alpha_0 = 137.5^\circ$). As a second sequence with small N_{PT} , we notice a sequence for $\alpha_0 \simeq 0.28$ ($2\pi\alpha_0 = 99.5^\circ$), the fifth row in Table 1, and (b) in Fig. 8. This sequence is observed but less commonly, and sometimes called the first accessory sequence. In general, the main sequence always sets the lower limit of N_{PT} , although there may be other sequences with the same lowest value.

In Fig. 9, N_{PT} for n_c up to 4, 5, 6, and 7 is plotted against α_0 . The figure indicates how the samples with different α_0 are discriminated as they grow. In the process of increasing n_c to 4, any sample for $1/3 < \alpha_0 < 1/2$ ($\Delta\alpha = 0.17$) is more favorable than that for $0 < \alpha_0 < 1/3$, because the former has a smaller value $N_{PT} = 2$ than the latter with $N_{PT} = 3$. As we increase n_c to 7 (the solid line in Fig. 9), only restricted samples within a narrow window $1/3 < \alpha_0 < 2/5$ ($\Delta\alpha = 0.07$) are favored because of

Table 1: Sequences of PF α resulting from arbitrarily chosen initial values of α_0 . N_{PT} in the last column counts the number of phyllotactic transitions (the number of times PF α changes) for $1 \leq n_c \leq 17$.

$\alpha_0 \backslash n_c$	1	2	3	4	5	6	7	8	9	10	11	13	17	N_{PT}
0.025714	1/2	1/3	1/4	1/5	1/6	1/7	1/8	1/9	1/10	1/11	1/12	1/14	1/18	16
0.104117	1/2	1/3	1/4	1/5	1/6	1/7	1/8	1/9	1/10	1/11	1/12	1/14	1/18	9
0.146317	1/2	1/3	1/4	1/5	1/6	1/7	1/8	1/9	1/10	1/11	1/12	1/14	1/18	7
0.175101	1/2	1/3	1/4	1/5	1/6	1/7	1/8	1/9	1/10	1/11	1/12	1/14	1/18	7
0.281978	1/2	1/3	1/4	1/5	1/6	1/7	1/8	1/9	1/10	1/11	1/12	1/14	1/18	5
0.286878	1/2	1/3	1/4	1/5	1/6	1/7	1/8	1/9	1/10	1/11	1/12	1/14	1/18	6
0.305352	1/2	1/3	1/4	1/5	1/6	1/7	1/8	1/9	1/10	1/11	1/12	1/14	1/18	6
0.375791	1/2	1/3	1/4	1/5	1/6	1/7	1/8	1/9	1/10	1/11	1/12	1/14	1/18	5
0.437801	1/2	1/3	1/4	1/5	1/6	1/7	1/8	1/9	1/10	1/11	1/12	1/14	1/18	6
0.469168	1/2	1/3	1/5	1/5	1/7	1/7	1/9	1/9	1/11	1/11	1/13	1/15	1/32	9

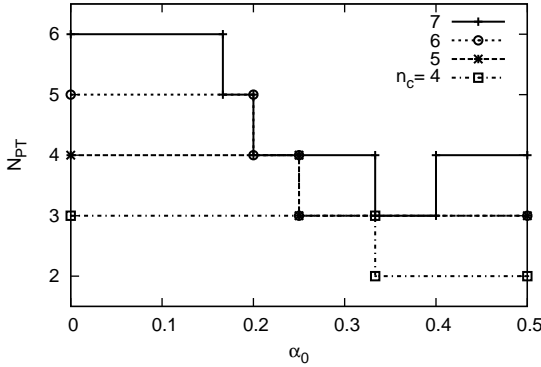


Figure 9: The number of phyllotactic transitions N_{PT} for $n_c = 4, 5, 6,$ and 7 are drawn against α_0 . As n_c increases to 7 , initial values α_0 within $1/3 < \alpha_0 < 2/5$ ($\Delta\alpha = 0.07$) are specifically selected because N_{PT} is the smallest there.

$N_{\text{PT}} = 3$, which is the lowest value for $n_c = 7$. In this filtering process, the width $\Delta\alpha$ for α_0 decreases rapidly as n_c increases. In Fig. 10, we plot N_{PT} against α_0 and n_c . The figure indicates that the minimum of N_{PT} with a decreasing width $\Delta\alpha$ develops around $\alpha_0 \simeq 0.38$ ($2\pi\alpha_0 = 137.5^\circ$) as n_c increases. In the end, a single value is selected for α_0 , namely, the golden angle $\alpha_0 = (3 - \sqrt{5})/2 \simeq 0.381966$ ($\Delta\alpha \rightarrow 0$).

In Fig. 11, we plot N_{PT} for n_c up to 20 and 50 , indicating how the stepwise ridges and troughs of N_{PT} develop as n_c increases. As n_c increases, α_0 should be gradually trapped in a minimum of N_{PT} . We find a small and shallow local minimum around $\alpha_0 \simeq 0.22$ ($2\pi\alpha_0 = 78^\circ$), besides the absolute minimum at $\alpha_0 \simeq 0.38$ and the first accessory $\alpha_0 \simeq 0.28$ mentioned above. These three cases are collectively called normal phyllotaxis (Sec. 3.5 and (B.13)). It is remarked that N_{PT} (or N_{PT}/n_c) becomes singular in the limit $n_c \rightarrow \infty$, for all the steps are subdivided and the widths of the steps shrink without limit as n_c increases. This is clear from Fig. 12, in which $n(\alpha_0) \equiv N_{\text{PT}}/n_c$ is

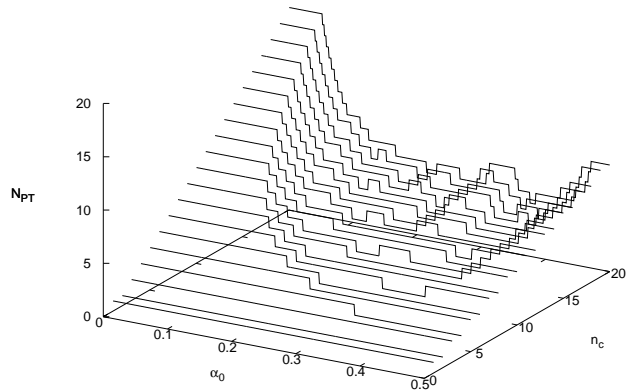


Figure 10: N_{PT} as a function of α_0 for $1 \leq n_c \leq 20$ (cf. Fig. 9). A narrow trough develops around $\alpha_0 \simeq 0.38$ ($2\pi\alpha_0 = 137.5^\circ$), as n_c increases.

plotted for $n_c = 100$ and 500 . Note that $n(\alpha_0)$ is minimized at the golden angle. But, from the figure, it appears almost impossible to reach the golden angle continuously by variational optimization. In our static mechanism, the golden angle is singled out through the screening process.

In Figs. 13 and 14, the range of α_0 within which the number N_{PT} is the smallest for given n_c is filled with the solid horizontal bar. It is clearly shown that several values are specifically favored for α_0 . Among others, we remark that the golden angle $2\pi\alpha_0 \simeq 137.5^\circ$ ($\alpha_0 \simeq 0.382$) is singled out for n_c near but less than the Fibonacci numbers in (13). The accuracy $\Delta\alpha$ for the golden angle converges rapidly, as mentioned above. We have $\Delta\alpha = 1/15$ for $n_c = 7$ in Fig. 9, and $\Delta\alpha = 1/1870$ around $n_c \simeq 85$ (cf. Table B.3).

To conclude, we may regard the hypothesis (H) as a law of phyllotaxis. In plain words, the Fibonacci phyllotaxis with the main sequence is favorably singled out because of

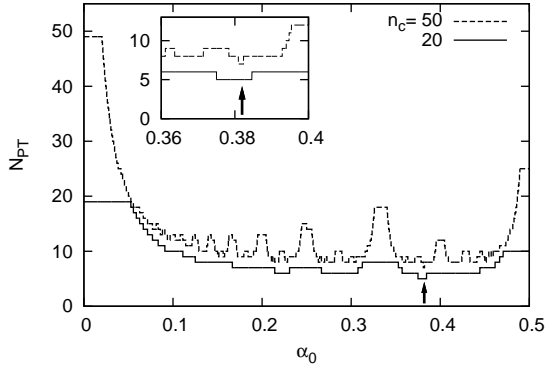


Figure 11: N_{PT} for $n_c = 20$ (solid line) and 50 (dashed line). The arrow at the minimum of N_{PT} indicates the golden angle $\alpha_0 \simeq 0.3820$ ($2\pi\alpha = 137.5^\circ$).

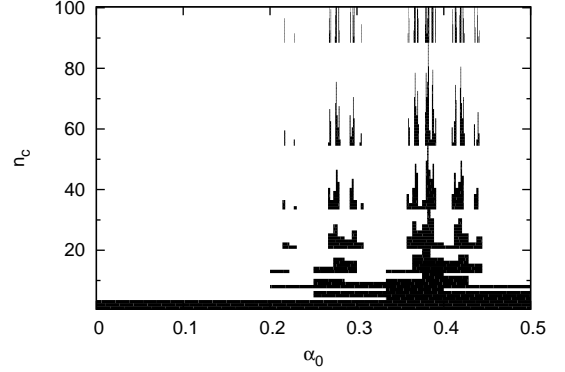


Figure 13: The range of α_0 within which N_{PT} takes the smallest value for given n_c is filled with horizontal bars, thereby favorable values for α_0 are pointed by ‘tapering needles’. They are $\alpha_0 \simeq 0.38, 0.28, 0.22$ (normal phyllotaxis), $\alpha_0 \simeq 0.42, 0.44$, and also $\alpha_0 \simeq 0.30, 0.37$ (cf. Sec. 3.5). The golden angle $\alpha_0 \simeq 0.38$ ($2\pi\alpha_0 = 137.5^\circ$) is singled out for $n_c \simeq 20, 30, 50, 80$.

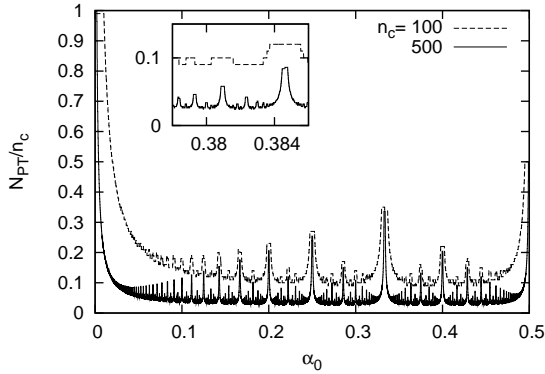


Figure 12: N_{PT}/n_c for $n_c = 100$ (dashed line) and 500 (solid line). The minimum at $\alpha_0 \simeq 0.38197$ is indiscernible for $n_c = 500$ ($\Delta\alpha \simeq 10^{-5}$).

its special stability against inevitable structural changes expected in the growing process.

3.4. Mathematics

The main results presented above are obtained directly from simple numerical analysis as shown in Fig. 3. Indeed it is straightforward to check them by hand when n_c is small, but it soon gets complicated as n_c becomes large. Mathematical analysis helps us not only to derive useful formula but also to deepen understanding of the mathematical structure of the problem. In particular, it is helpful for us to have analytical expressions of $(n_0, \Delta n)$ and $\Delta\alpha$ for PFs belonging to typical sequences found in nature. The mathematical analysis is indispensable if we do not content ourselves with several specific circumstances of lower phyllotaxis. Mathematical results are delegated to the appendixes. Here we point out only that Fig. 4 has the same structure as the *Stern-Brocot tree* of number theory ([9]), which contains each rational numbers exactly once. Relations between numbers in the tree are concisely repre-

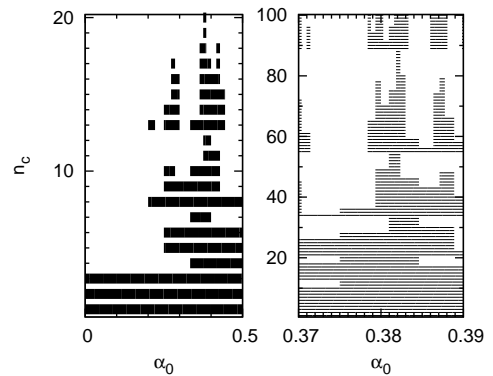


Figure 14: The range of α_0 for the least N_{PT} is filled with horizontal lines (Fig. 13 enlarged vertically and horizontally).

sented in terms of *mediants* (Appendix A) and *continued fractions* (Appendix B).

3.5. Sequences

As given in Table 1, a general phyllotactic pattern derived from a random value of α_0 does not fit in with observed regularity. Indeed, if PT would have to occur too frequently, the concepts of the PF and PT themselves could become indefinite. As a matter of fact, fortunately, observed sequences come around with astonishing regularity. Only several types of sequences exist in nature. For the purpose of classifying the observed sequences, one often adopts a tacit theoretical procedure of inferring a mathematical limit α of a given sequence by extrapolation. The limit divergence α , generally an irrational number, is then used to represent the sequence. However, it must be kept in mind that any phyllotactic sequence does terminate finitely in practice, and inferring a limit from a finite sequence may be problematic. Be that as it may, a sequence of principal convergents of a noble number (Eq. (B.9)) has been a central subject. We can assess frequencies of occurrence of various sequences quantitatively by comparing N_{PT} for the sequences. Below we use a shorthand bracket notation for a sequence given in a paragraph below Eq. (B.14) in Appendix B.

The main sequence with the limit divergence $\alpha_0 = 0.382$ ($2\pi\alpha_0 = 137.5^\circ$) is given by

$$[2] : 1/2, 1/3, 2/5, 3/8, 5/13, 8/21, 13/34, 21/55, \dots \quad (14)$$

The first accessory sequence with the limit $\alpha_0 = 0.276$ ($2\pi\alpha_0 = 99.5^\circ$) is

$$[3] : 1/2, 1/3, 1/4, 2/7, 3/11, 5/18, 8/29, 13/47, \dots$$

The second accessory sequence for $\alpha_0 = 0.217$ ($2\pi\alpha_0 = 78.0^\circ$) is

$$[4] : 1/2, 1/3, 1/4, 1/5, 2/9, 3/14, 5/23, 8/37, \dots$$

These are called normal phyllotaxis. As an example of anomalous phyllotaxis, the first lateral sequence for $\alpha_0 = 0.420$ ($2\pi\alpha_0 = 151.1^\circ$) is

$$[2, 2] : 1/2, 1/3, 2/5, 3/7, 5/12, 8/19, 13/31, 21/50, \dots$$

In addition, we can think of the sequence for $\alpha_0 = 0.296$ ($2\pi\alpha_0 = 106.4^\circ$),

$$[3, 2] : 1/2, 1/3, 1/4, 2/7, 3/10, 5/17, 8/27, 13/44, \dots$$

And, for $\alpha_0 = 0.367$ ($2\pi\alpha_0 = 132.2^\circ$),

$$[2, 1, 2] : 1/2, 1/3, 2/5, 3/8, 4/11, 7/19, 11/30, 18/49, \dots$$

There is controversy concerning the existence of the last two sequences ([27, 11]). As the general fact of observation, any other sequence than the main sequence [2] may be regarded as exceptional.

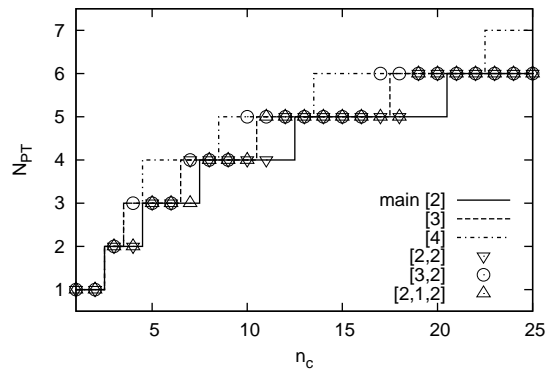


Figure 15: N_{PT} is plotted against n_c for major sequences. The sequences with the limit index $\alpha_0 \simeq 0.38, 0.28, 0.22, 0.42, 0.30$ and 0.37 are represented as [2], [3], [4], [2,2], [3,2] and [2,1,2], respectively. The main sequence [2] sets the lower limit of N_{PT} .

For these sequences, N_{PT} is plotted against n_c in Fig. 15. The main sequence always sets the lower limit of N_{PT} . At $n_c = 4$, [2,2] and [2,1,2] have $N_{PT} = 2$, and the others have $N_{PT} = 3$. This is because the first three terms of [2,2] and [2,1,2] (up to $2/5$) are the same as the main sequence [2]. From around $n_c = 10$, the priority order of occurrence of the sequences is inferred as [2,2], [3], [3,2], and [4]. For such small n_c as shown in Fig. 15, the order of [2,1,2] and [2,2] cannot be decided uniquely. Note that [3,2] and [2,1,2] may be regarded as satellite sequences of [3] and [2], respectively. This is seen from Fig. 13. Therefore, according to our result, extraordinary [3,2] and [2,1,2] are less unlikely than [4] of ‘normal’ phyllotaxis. In Table 2, for general sequences, we tabulate the values of n_c at which N_{PT} is minimized. Many sequences become favorable when n_c is equal to a Fibonacci number in (13). This is clear from Fig. 13. We find that normal phyllotaxis of higher order [n] ($n = 4, 5, \dots$) appears not so specially preferable as widely supposed. In fact, Fig. 13 indicates that N_{PT} has no absolute minimum for $0 < \alpha_0 < 0.2$ and $n_c \geq 4$ ($\alpha_0 = 0.178$ for [5] and $\alpha_0 = 0.151$ for [6]). A low-order sequence with [l, m, n] ($l, m, n \leq 3$) looks rather favorable.

The order in the frequency of occurrence is generally consistent with the available data, though the number of observations is still too limited to draw a definite conclusion ([7, 11]).

4. Discussion

We have made full use of an important result of our model that the phyllotactic index α is given by a fraction. As a problem of macroscopic physics, it goes without saying that this is but a good approximation and mathematical rigor should not be expected in this respect. In this section, we investigate the effect of the lateral width X of the interaction $V(x)$ in Eq. (2). There is an optimal value

Table 2: Table for the growth index n_c at which a given sequence makes a pattern with the minimum N_{PT} . In the first row, the minimum value N_{PT} is given. The main sequence [2]: (1,2) covers all integers for n_c ($N_{PT} = 2$ for $n_c = 3, 4$, etc.). The bracket notation for the sequence in the first column is explained in a paragraph below Eq. (B.14). (A pair of numbers in the round bracket are parastichy pairs, i.e., seed values for a Fibonacci recurrence relation.)

N_{PT}	2	3	4	5	6	7	8	9
[2] : (1, 2)	3,4	5-7	8-12	13-20	21-33	34-54	55-88	89-143
[3] : (1, 3)	3	5,6	8-10	13-17	21-28	34-46	55-75	89-122
[4] : (1, 4)	3		8	13	21,22	34-36	55-59	89-96
[5] : (1, 5)	3							
[2, 2] : (2, 5)	3,4	5,6	8-11	13-18	21-30	34-49	55-80	89-130
[2, 3] : (2, 7)	3,4	5,6	8	13-15	21-24	34-40	55-65	89-106
[2, 4] : (2, 9)	3,4	5,6	8					
[3, 2] : (3, 7)	3	5,6	8,9	13-16	21-26	34-43	55-70	89-114
[3, 3] : (3, 10)	3	5,6	8,9		21,22	34,35	55-58	89-94
[3, 4] : (3, 13)	3	5,6	8,9					
[4, 2] : (4, 9)	3		8		21	34	55,56	89-91
[4, 3] : (4, 13)	3		8					
[2, 1, 2] : (3, 8)	3,4	5-7	8-10	13-18	21-29	34-48	55-78	89-127
[2, 1, 3] : (3, 11)	3,4	5-7	8-10	13	21-24	34-38	55-63	89-102
[2, 1, 4] : (3, 14)	3,4	5-7	8-10	13				
[2, 2, 2] : (5, 12)	3,4	5,6	8-11	13-16	21-28	34-45	55-74	89-120
[2, 2, 3] : (5, 17)	3,4	5,6	8-11	13-16	21	34-38	55-60	89-99
[2, 2, 4] : (5, 22)	3,4	5,6	8-11	13-16	21			
[2, 3, 2] : (7, 16)	3,4	5,6	8	13-15	21,22	34-38	55-61	89-100
[2, 3, 3] : (7, 23)	3,4	5,6	8	13-15	21,22			
[2, 3, 4] : (7, 30)	3,4	5,6	8	13-15	21,22			
[2, 4, 2] : (9, 20)	3,4	5,6	8					
[3, 1, 2] : (4, 11)	3	5,6	8-10	13,14	21-25	34-40	55-66	89-107
[3, 1, 3] : (4, 15)	3	5,6	8-10	13,14				
[3, 2, 2] : (7, 17)	3	5,6	8,9	13-16	21-23	34-40	55-64	89-105
[3, 2, 3] : (7, 24)	3	5,6	8,9	13-16	21-23			
[3, 3, 2] : (10, 23)	3	5,6	8,9		21,22		55	
[3, 3, 3] : (10, 33)	3	5,6	8,9		21,22			
[4, 1, 2] : (5, 14)	3		8	13				
[4, 1, 3] : (5, 19)	3		8	13				
[4, 2, 2] : (9, 22)	3		8		21			

\bar{X} for X around which α is given by a fraction, as expected. The optimal width \bar{X} may be used to see if a minimum of $v(\alpha)$ is really achieved practically. If the potential function $v(\alpha)$ is nearly constant and flat in a wide region around a minimum, it will take too long time to reach the true minimum because the torsional driving force $-\frac{dv(\alpha)}{d\alpha}$ toward the minimum, in the right-hand side of Eq. (5), becomes practically zero. This happens if $X \ll \bar{X}$, as shown in Fig. 16 for $X = 0.05$. It is known that the use of a fraction, as originally made by Schimper and Braun, is not always adequate ([8]).

To put it concretely, let us examine PF 3/8, which occurs in between 1/3 and 2/5. We consider

$$1/3 < \alpha < 2/5, \quad (15)$$

and

$$5 \leq n_c < 8. \quad (16)$$

Then, for $v(\alpha)$ in Eq. (9), all the other terms than $m = 3$ and $m = 5$ are effectively neglected, so that we get

$$\begin{aligned} v(\alpha) &\simeq v_3V(3\alpha) + v_5V(5\alpha) \\ &= v_3V(3\alpha - 1) + v_5V(5\alpha - 2), \end{aligned} \quad (17)$$

for $V(x)$ is periodic. In effect, this is a minimal model for PF 3/8. This may be interpreted as a mathematical expression of Hofmeister's rule, that new 'leaf' arises in the largest gap between the previous ones. Note, however, that we are not concerned with mechanical dynamics of phyllotaxis at the apex.

On the one hand, as a function of α , $V(3\alpha - 1)$ has a peak with the width $X/3$ at $\alpha = 1/3$, the lower boundary of (15). On the other hand, $V(5\alpha - 2)$ has a peak with the width $X/5$ at $\alpha = 2/5$, the upper boundary of (15). An optimal width \bar{X} is estimated by equating the total width $\bar{X}/3 + \bar{X}/5$ with the allowed range for α , that is, $\Delta\alpha = 2/5 - 1/3$. We obtain the result $\bar{X} = 1/8$ for 3/8.

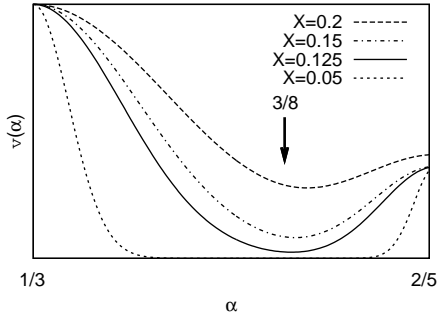


Figure 16: For various X around an optimal value $\bar{X} = 0.125$, the effective potential $v(\alpha)$ is plotted by using Eq. (2) and $v_n = 0.6^n$ for $n \leq n_c$ ($5 \leq n_c < 8$). For $X = 0.05$ ($\ll \bar{X}$), $v(\alpha)$ has a flat bottom for a wide range of α .

According to Eq. (3), the optimal angular width of interaction is $\Delta\theta \simeq 90^\circ$ for $3/8$. In the ideal case $X = \bar{X}$, $v(\alpha)$ has a minimum at $\alpha = 1/3 + \bar{X}/3 = 2/5 - \bar{X}/5 = 3/8$, as expected. The derivation outlined here indicates that the result will not depend on $V(\alpha)$ specifically.

We present Fig. 16 to show the effect of X on $v(\alpha)$. To draw the figure, we use a full form of $v(\alpha)$ and did not use the approximation in Eq. (17). In any case, the difference due to the approximation is negligible. As mentioned, for $X \simeq \bar{X}$, we obtain $\alpha \simeq 3/8$ properly with good accuracy. As X is decreased from \bar{X} , $v(\alpha)$ around the minimum gets flattened. As a matter of practical fact, the minimum would not be reached in the extreme case of $X \ll \bar{X}$. When $X < \bar{X}$, there appears a flat region in

$$\frac{1}{3} + \frac{X}{3} < \alpha < \frac{2}{5} - \frac{X}{5}, \quad (18)$$

the width of which is $\Delta\alpha_{\text{flat}} = (1 - 8X)/15 = (1 - \frac{X}{\bar{X}})/15$. This is smaller than the full width $\Delta\alpha = 1/15$ of (15), as it should be. In practice, insofar as α stays within the flat region, we may rather observe the primary angle $\alpha = \alpha_0$ as it is, since the secondary torsion is not effective any longer.

In general, the optimal width \bar{X} for a fraction p/q is given by $\bar{X} = 1/q$, and the width of the flat region is

$$\Delta\alpha_{\text{flat}} = \left(1 - \frac{X}{\bar{X}}\right) \Delta\alpha, \quad (19)$$

for $X < \bar{X}$ (Appendix C). As we follow any sequence up in the tree of Fig. 4, the denominator q_n of PF $\alpha = p_n/q_n$ stays constant or increases, so that \bar{X} is constant or decreases. In effect, it decreases roughly as $\bar{X} \sim 1/n_c$. By contrast, the model parameter X should be fit with a real plant. Consequently, the condition $X < \bar{X}$ may hold in early few terms of a sequence (namely, $1/2, 1/3$, etc., when n_c is small). Then we could no more expect to observe these low order PFs. We rather observe an inherent value $\alpha = \alpha_0$ so far as it falls within a flat region with the width $\Delta\alpha_{\text{flat}}$. This is consistent with observations.

5. Conclusions

With the aid of biological hypotheses, we showed that prevalent sequences of phyllotactic fractions are satisfactorily explained by a physical model of plant growth. The model has interesting mathematical properties. Among others, we bring to light a Stern-Brocot type number-theoretical structure that has been unnoticed thus far in this field. To extract the mathematical essence of the phenomenon, we have to base our theory on the abstract model by discarding real biological implementation as non-essential details. According to the proposed static mechanism, the phyllotactic pattern with the main Fibonacci sequence is naturally selected because it entails the least number of phyllotactic structural transitions while growing to a mature plant.

Acknowledgement

I wish to express my appreciation to the reviewer for the invaluable comments which helped me improve the paper significantly.

References

- [1] Adler, I., 1974. A model of contact pressure in phyllotaxis. *J. Theor. Biol.* 45, 1.
- [2] Adler, I., Barabé, D., Jean, R. V., 1997. A history of the study of phyllotaxis. *Ann. Bot.* 80, 231.
- [3] Bryntsev, V. A., 2004. Types of phyllotaxis and patterns of their realization. *Russ. J. Dev. Biol.* 2, 114.
- [4] Coxeter, H. S. M., 1961. *Introduction to Geometry*. Wiley, New York and London.
- [5] Coxeter, H. S. M., 1972. The role of intermediate convergents in tait's explanation for phyllotaxis. *J. Algebra* 20, 167.
- [6] Douady, S., Couder, Y., 1996. Phyllotaxis as a dynamical self organizing process part I: The spiral modes resulting from time-periodic iterations. *J. Theor. Biol.* 178, 255.
- [7] Fujita, T., 1937. Über die Reihe 2,5,7,12... in der schraubigen Blattstellung und die mathematische Betrachtung verschiedener Zahlenreihensysteme. *Bot. Mag. Tokyo* 51, 298.
- [8] Fujita, T., 1939. Statistische Untersuchungen über den Divergenzwinkel bei den schraubigen Organstellungen. *Bot. Mag. Tokyo* 53, 194.
- [9] Graham, R. L., Knuth, D. E., Patashnik, O., 1994. *Concrete Mathematics: A Foundation for Computer Science*. Reading, Massachusetts: Addison-Wesley.
- [10] Hellwig, H., Neukirchner, T., 2010. Phyllotaxis. *Math. Semesterber.* 57, 17.
- [11] Jean, R. V., 1994. *Phyllotaxis: A Systemic Study in Plant Morphogenesis*. Cambridge Univ. Press, Cambridge, New York.
- [12] Kuhlmeier, C., 2007. Phyllotaxis. *TRENDS in Plant Science* 12, 143.
- [13] Larson, P. R., 1977. Phyllotactic transitions in the vascular system of *Populus deltoides* Bartr. as determined by ^{14}C labeling. *Planta* 134, 241.
- [14] Levitov, L. S., 1991. Energetic approach to phyllotaxis. *Europhys. Lett.* 14, 533.
- [15] Marzec, C., Kappraff, J., 1983. Properties of maximal spacing on a circle related to phyllotaxis and to the golden mean. *J. Theor. Biol.* 103, 201.
- [16] Richards, F. J., 1951. Phyllotaxis: Its quantitative expression and relation to growth in the apex. *Philos. Trans. R. Soc. B* 225, 509.

- [17] Ridley, J. N., 1982. Packing efficiency in sunflower heads. *Math. Biosci.* 58, 129.
- [18] Rivier, N., Occelli, R., Pantaloni, J., Lissowski, A., 1984. Structure of Bénard convection cells, phyllotaxis and crystallography in cylindrical symmetry. *J. Phys. (Paris)* 45, 49.
- [19] Rothen, F., Koch, A. J., 1989. Phyllotaxis, or the properties of spiral lattices. I. shape invariance under compression. *J. Phys. (Paris)* 50, 633.
- [20] Rothen, F., Koch, A. J., 1989. Phyllotaxis or the properties of spiral lattices. II. packing of circles along logarithmic spirals. *J. Phys. (Paris)* 50, 1603.
- [21] Schimper, K. F., 1835. Beschreibung des Symphytum Zeyheri und seiner zwei deutschen verwandten der S.bulbosum Schimper und S. tuberosum Jacq. Winter.
- [22] Schwendener, S., 1878. Mechanische Theorie der Blattstellungen. Leipzig: Engelmann.
- [23] Snow, M., Snow, R., 1962. A theory of the regulation of phyllotaxis based on *Lupinus albus*. *Philos. Trans. Roy. Soc. London B* 244, 483.
- [24] Thompson, D. W., 1917. On Growth and Form. Oxford. Clarendon Press.
- [25] Thornley, J. H. M., 1975. Phyllotaxis. I. A Mechanistic Model. *Ann. Bot.* 39, 491.
- [26] van Iterson, G., 1907. Mathematische und Mikroskopisch-Anatomische Studien über Blattstellungen. Jena.
- [27] Zagórska-Marek, B., 1994. Phyllotactic diversity in *Magnolia* flowers. *Acta Soc. Bot. Poloniae* 63, 117.

Appendix A. Mediant

The *mediant* of two fractions m/n and p/q is given by $(m+p)/(n+q)$, where m and n (p and q) are relatively prime integers. Let us call m/n and p/q as parent fractions of a child fraction $(m+p)/(n+q)$.

The Stern-Brocot tree of fractions between 0 and $1/2$ is obtained by the following operation ([9]). Start from the initial fractions $0/1(=0)$ and $1/2$. Repeat inserting the mediant of two adjacent fractions, and arranging them in numerical order. The first mediant is $1/3$ between $0/1$ and $1/2$, and they are arranged as $(0/1)$, $1/3$, $(1/2)$. In the second order, we obtain $1/4$ between $0/1$ and $1/3$, and $2/5$ between $1/3$ and $1/2$. They are arranged as $(0/1)$, $1/4$, $(1/3)$, $2/5$, $(1/2)$. In the third order, we obtain $(0/1)$, $1/5$, $(1/4)$, $2/7$, $(1/3)$, $3/8$, $(2/5)$, $3/7$, $(1/2)$. Here we put the fractions in the previous orders in parentheses. The Stern-Brocot tree has been anticipated by Schimper ([21, 10]).

Our tree in Fig. 4 is related to but not the same as the Stern-Brocot tree. As an important difference, we have to order fractions by the growth index n_c . In other words, we need to know $(n_0, \Delta n)$ of the fractions. For instance, let us consider $2/5$. For $n_c = 3$ in Fig. 4, $(m+p)/(n+q) = 2/5$ is the mediant of $p/q = 1/3$ and $m/n = 1/2$ ($m = 1, n = 2, p = 1, q = 3$). By ordering the fractions according to the denominators, q and n , let us call $p/q = 1/3$ and $m/n = 1/2$ as the younger and the older parent of $2/5$. On the one hand, the mediant $2/5$ is born when the younger parent $p/q = 1/3$ dies at $n_c = q = 3$. On the other hand, $2/5$ dies at $n_c = n+q = 5$, the denominator of $2/5$. Therefore, we obtain $3 \leq n_c < 5$ and $\Delta n = 1$ for $2/5$. In general, the mediant $(m+p)/(n+q)$ of m/n and p/q ($n < q$) has

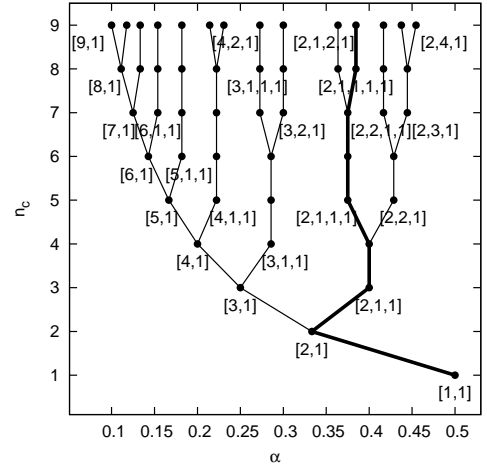


Figure A.17: The branching structure in Fig. 4 is schematically shown (a) for $p/q < m/n$ and (b) for $p/q > m/n$, where m and n , p and q are relatively prime numbers satisfying $n < q$. In both cases, two daughter fractions $(m+2p)/(n+2q)$ and $(2m+p)/(2n+q)$ at the top of the figure are derived from a mother fraction $(m+p)/(n+q)$ in the middle. The mother $(m+p)/(n+q)$ is derived as a child of the parents p/q and m/n . We obtain $\Delta n = q - 1$ for $(m+2p)/(n+2q)$, and $\Delta n = n - 1$ for $(2m+p)/(2n+q)$ and $(m+p)/(n+q)$. The path to increase Δn traces the bold zigzag line.

$q \leq n_c < n+q$. For $(m+p)/(n+q)$ ($n < q$), we obtain

$$(n_0, \Delta n) = (q, n - 1). \quad (\text{A.1})$$

Next we consider $\Delta\alpha$. In order to realize $\alpha = (m+p)/(n+q)$, α_0 has to lie between the parents m/n and p/q , and we get $\Delta\alpha = |\frac{m}{n} - \frac{p}{q}|$. The parent fractions belonging to the tree are shown to satisfy $|mq - np| = 1$ ([9]). Hence we conclude

$$\Delta\alpha = \frac{1}{nq} \quad (\text{A.2})$$

for $(m+p)/(n+q)$. These formulas may be used for Fig. 5.

For the hypothesis (H) in Sec. 3.3, we have to compare Δn of two daughter fractions derived from a mother fraction in Fig. 4. (We tell a mother-daughter relation from a parent-child relation.) Consider $(m+p)/(n+q)$ as a mother fraction, derived as a child of parents m/n and p/q ($n < q$) (Fig. A.17). One daughter fraction $(2m+p)/(2n+q)$ occurs between $(m+p)/(n+q)$ and m/n . The other daughter fraction $(m+2p)/(n+2q)$ occurs between $(m+p)/(n+q)$ and p/q . On account of Eq. (A.1), the former $(2m+p)/(2n+q)$ has $(n_0, \Delta n) = (n+q, n-1)$, whereas the latter $(m+2p)/(n+2q)$ has $(n_0, \Delta n) = (n+q, q-1)$. By assumption $n < q$, the daughter fraction $(m+2p)/(n+2q)$ has the larger $\Delta n = q - 1$ than $(2m+p)/(2n+q)$ with $\Delta n = n - 1$. For two daughter fractions derived from a mother fraction, the one with a larger denominator always increases Δn , whereas the other does not change Δn from the mother fraction.

This rule is read from Fig. 5. At every branching point (node), one branch grows to the right to increase Δn . The

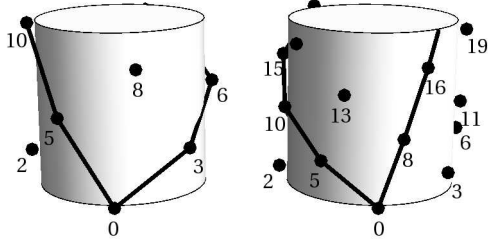


Figure A.18: Patterns with the same divergence angle $\alpha = 0.38$ appear to have different parastichy pairs $(n, q) = (3, 5)$ (left) and $(5, 8)$ (right), depending on a vertical length scale. The 5-parastichy winds up clockwise. Thus this ‘transition’ of a parastichy pair is a superficial phenomenon. The apparent change from $(3, 5)$ to $(5, 8)$ is called rising phyllotaxis. Rising phyllotaxis restricts a range allowed for α (Fig. A.19).

other goes down along the ordinate in the main figure. According to (H), the sequence with ever increasing Δn comprises the most favorable branch of our evolutionary tree. A favored sequence in the tree diagram of Fig. 4 traces a zigzag path as depicted with the bold line in Fig A.17. This result may be compared with a dynamical counterpart (Appendix B, Appendix C).

In practice, when the divergence angle α deviates from an exact fraction, a pair of integers (n, q) , called a *parastichy pair*, is used to represent a phyllotactic pattern consisting of most conspicuously visible families of n and q secondary spirals (parastichies) crossing with each other. A q -parastichy is a secondary spiral running through the points (p, θ_p) , $(p+q, \theta_{p+q})$, $(p+2q, \theta_{p+2q})$, $(p+3q, \theta_{p+3q})$, etc., where $p = 0, 1, 2, \dots, q-1$ (Fig. A.18). To derive a parastichy pair for given α is a purely geometrical problem ([1, 11]). In our tree system, we find a simple result that *we obtain a visible parastichy pair (n, q) when α lies between two neighboring (parent) fractions m/n and p/q in our tree.* Accordingly, PF $\alpha = (m+p)/(n+q)$ may be replaced by the parastichy pair (n, q) . In place of Fig. 7, we obtain Fig. A.19, which may be useful to analyze real systems.

Appendix B. Continued Fraction

A real number α ($0 < \alpha < 1$) is represented as a *continued fraction*,

$$\alpha = \frac{1}{a_1 + \frac{1}{a_2 + \frac{1}{a_3 + \dots}}} \equiv [a_1, a_2, a_3, \dots], \quad (\text{B.1})$$

where a_i ($i = 1, 2, \dots$) is a positive integer. Every rational number has two continued fraction expansions. In one the final term is 1, that is, a rational number α is represented finitely as $\alpha = [a_1, a_2, \dots, a_n, 1]$. For an irrational number α , there is a successive rational approximation, $p_n/q_n = [a_1, \dots, a_n]$ ($n = 1, 2, \dots$), in terms of relatively

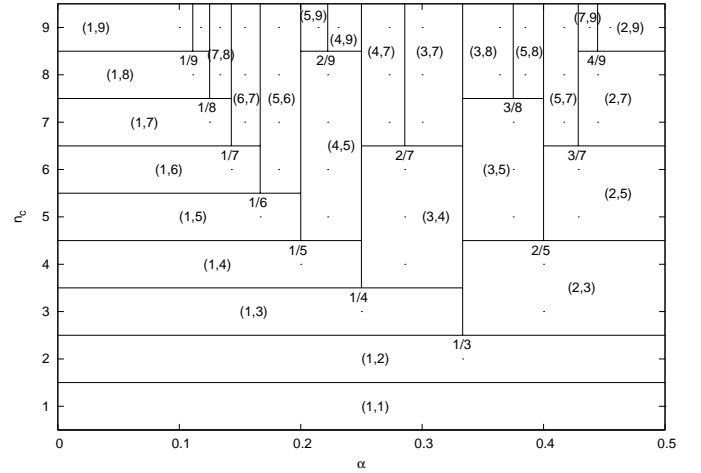


Figure A.19: Diagram of a phyllotactic system with one genetic spiral, showing the visible opposed parastichy pair (n, q) . For $3/8 < \alpha < 2/5$, we may obtain $(1, 2)$, $(2, 3)$, $(3, 5)$ or $(5, 8)$, depending on a vertical length scale (Fig. A.18). Conversely, if we observe rising phyllotaxis through parastichy pairs $(1, 2)$, $(2, 3)$, $(3, 5)$ and $(5, 8)$, then the divergence angle α must meet the constraint $3/8 < \alpha < 2/5$ ($\Delta\alpha = 0.025$). For a system with J genetic spirals, α and (n, q) are replaced by $J\alpha$ and $J(n, q)$, respectively.

prime positive integers p_n and q_n satisfying the recursion relations,

$$p_{n+2} = a_{n+2}p_{n+1} + p_n, \quad (\text{B.2})$$

$$q_{n+2} = a_{n+2}q_{n+1} + q_n, \quad (\text{B.3})$$

and

$$p_0 = 0, p_1 = 1, q_0 = 1, q_1 = a_1. \quad (\text{B.4})$$

The fraction p_n/q_n ($n = 1, 2, \dots$) is called a *principal convergent* of α . The difference between successive principal convergents is given by

$$\frac{p_{n+1}}{q_{n+1}} - \frac{p_n}{q_n} = \frac{(-1)^n}{q_n q_{n+1}}, \quad (\text{B.5})$$

and α lies between even and odd order convergents,

$$\frac{p_{2k}}{q_{2k}} < \alpha < \frac{p_{2k+1}}{q_{2k+1}}. \quad (\text{B.6})$$

Thus the principal convergent p_n/q_n approaches to the limit α in a zigzag manner.

In terms of the bracket notation defined in Eq. (B.1), we obtain Fig. B.20 in place of Fig. 4. From the figure, we immediately notice the bifurcation rule holding at every node,

$$[a_1, a_2, \dots, a_n, 1] \longrightarrow \frac{[a_1, a_2, \dots, a_n, 1, 1]}{[a_1, a_2, \dots, a_n + 1, 1]}. \quad (\text{B.7})$$

It is easily checked that the upper branch in (B.7) increases Δn , and the lower one conserves Δn (Appendix A). Therefore, according to (H) in Sec. 3.3, it is particularly important for us to study the following sequence of fractions

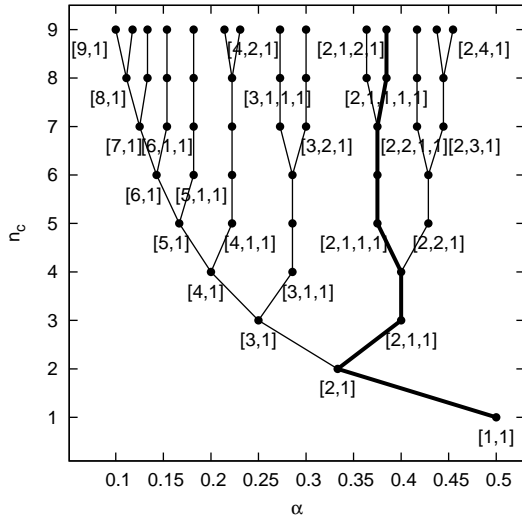


Figure B.20: Fractions in Fig. 4 are represented with the bracket notation for continued fractions defined in Eq. (B.1).

($a_i \neq 1$ for $i = 1, 2, \dots, n$):

$$\begin{aligned} & [a_1, a_2, \dots, a_n, 1], \\ & [a_1, a_2, \dots, a_n, 1, 1], \\ & [a_1, a_2, \dots, a_n, 1, 1, 1], \\ & [a_1, a_2, \dots, a_n, 1, 1, 1, 1], \dots \end{aligned} \quad (\text{B.8})$$

These are comprised in the principal convergents of a *noble number*,

$$\alpha_{\text{noble}} = [a_1, a_2, \dots, a_n, 1, 1, 1, 1, \dots]. \quad (\text{B.9})$$

Owing to the succession of $a_i = 1$ ($i > n$), for a sequence of fractions p_n/q_n on a favored branch according to (H), the numerator p_n and denominator q_n obey the Fibonacci recursion relations $p_n = p_{n-1} + p_{n-2}$ and $q_n = q_{n-1} + q_{n-2}$.

A sequence of principal convergents of a noble number has been given a special status in theoretical studies of phyllotaxis ([5, 15, 18, 19]). The most important is the golden angle (per 2π) for $a_1 = 2$ and $a_n = 1$ ($n = 1, 2, 3, \dots$),

$$\alpha = [2, 1, 1, 1, \dots] = 1/(2 + \tau^{-1}) = \tau^{-2} = (3 - \sqrt{5})/2, \quad (\text{B.10})$$

where the golden ratio τ is given by

$$\tau = 1 + [1, 1, 1, \dots] = (\sqrt{5} + 1)/2, \quad (\text{B.11})$$

or

$$\tau^{-1} = [1, 1, 1, \dots] = (\sqrt{5} - 1)/2. \quad (\text{B.12})$$

In the literature, a sequence is referred to in several ways. In particular, a sequence with a limit index

$$\alpha = [t, 1, 1, 1, \dots] = 1/(t + \tau^{-1}) \quad (\text{B.13})$$

($t = 2, 3, \dots$) is called *normal phyllotaxis*. The main sequence for Eq. (B.10) corresponds to the special case $t = 2$. The cases $t = 3$ and $t = 4$ are called the first and the second *accessory sequence*, respectively. On the other side, a sequence with a limit angle

$$\alpha = [2, t, 1, 1, 1, \dots] = 1/(2 + (t + \tau^{-1})^{-1}), \quad (\text{B.14})$$

($t = 2, 3, \dots$) is sometimes called the *lateral sequence*.

For convenience sake, let us introduce another concise notation. To denote a whole sequence with a limit of

$$\alpha = [a_1, a_2, \dots, a_n, 1, 1, \dots] = 1/(a_1 + (a_2 + (\dots + (a_n + \tau^{-1})^{-1})^{-1})^{-1}) \quad (\text{B.15})$$

we simply reuse a symbol for a continued fraction $[a_1, a_2, \dots, a_n]$ ($a_n \neq 1$). Hence the main sequence is

$$[2] : 1/2, 1/3, 2/5, 3/8, 5/13, 8/21, 13/34, 21/55, \dots \quad (\text{B.16})$$

To obtain the sequence $[3, 2]$ with a limit $\alpha = 1/(3 + (2 + \tau^{-1})^{-1})$, collect the fractions from $1/2$ to $[3, 2] = 2/7$ up along the tree in Fig. 4, namely, $1/2, 1/3, 1/4, 2/7$. Then, from the daughter fractions $3/10$ and $3/11$ of $2/7$, choose the unfavorable one with a smaller denominator, namely, $3/10$. After them follow all the fractions on the favorable branch ramifying from $3/10$, namely, $5/17, 8/27, 13/44, 21/71, 34/115, 55/186, 89/301, \dots$. As noted below Eq. (B.9), these obey the Fibonacci recursion relation (e.g., $13/44 = (5+8)/(17+27)$). To summarize, we obtain

$$[3, 2] : 1/2, 1/3, 1/4, 2/7, 3/10, 5/17, 8/27, 13/44, 21/71, 34/115, \dots$$

Major sequences are given in Sec. 3.5.

A sequence is commonly represented by parastichy numbers instead of fractions. Translation is made without difficulty by noticing the denominators (Appendix A).

$$[2] : (1, 1), (1, 2), (2, 3), (3, 5), (5, 8), (8, 13), (13, 21), \dots \quad (\text{B.17})$$

$$[3, 2] : (1, 1), (1, 2), (1, 3), (3, 4), (3, 7), (7, 10), (10, 17), (17, 27), \dots \quad (\text{B.18})$$

We may combine repeated numbers on favored branches.

$$[2] : 1, 2, 3, 5, 8, 13, 21, \dots \quad (\text{B.19})$$

$$[3, 2] : (1, 2), (1, 3, 4), (3, 7, 10, 17, 27, \dots) \quad (\text{B.20})$$

All but the last branch may be omitted.

$$[3, 2] : 3, 7, 10, 17, 27, \dots \quad (\text{B.21})$$

Most concisely, only the first two numbers may be given as seed values of recurrence.

$$[2] : (1, 2). \quad (\text{B.22})$$

$$[3, 2] : (3, 7). \quad (\text{B.23})$$

In this notation, typical sequences are generally given as follows (cf. Table 2).

$$[a] : (1, a). \quad (a = 2, 3, \dots) \quad (\text{B.24})$$

$$[p, a] : (p, ap + 1). \quad (a, p = 2, 3, \dots) \quad (\text{B.25})$$

$$[p - 1, 1, a - 1] : (p, ap - 1). \quad (a, p = 3, 4, \dots) \quad (\text{B.26})$$

$$[p - 1, 2, a - 1] : (2p - 1, a(2p - 1) - p). \quad (a, p = 3, 4, \dots) \quad (\text{B.27})$$

According to [7], the first sequence system $[a]$ is common, the second sequence system $[p, a]$ is rarely observed, and the third sequence system $[p - 1, 1, a - 1]$ is extremely rare. This is consistent with our results in Table 2.

Now our task is to get $\Delta\alpha$ and $(n_0, \Delta n)$ for a sequence of principal convergents of a noble number. From Eq. (B.5), we get

$$\frac{p_n}{q_n} - \frac{p_{n-1}}{q_{n-1}} = \frac{(-1)^{n-1}}{q_{n-1}q_n}, \quad (\text{B.28})$$

and

$$\frac{p_n}{q_n} - \frac{p_{n-2}}{q_{n-2}} = \frac{(-1)^n a_n}{q_n q_{n-2}}. \quad (\text{B.29})$$

These equations signify that p_n/q_n lies between p_{n-1}/q_{n-1} and p_{n-2}/q_{n-2} . We find that p_n/q_n has

$$\Delta\alpha = \left| \frac{p_{n-1}}{q_{n-1}} - \frac{p_{n-2}}{q_{n-2}} \right| = \frac{1}{q_{n-1}q_{n-2}}. \quad (\text{B.30})$$

According to our model, a child fraction p_n/q_n is born at $n_c = q_{n-1}$ from a parent fraction p_{n-1}/q_{n-1} , and dies at $n_c = q_n$. Hence, we obtain $q_{n-1} \leq n_c < q_n$ for p_n/q_n . Using Eq. (B.3), for p_n/q_n of a noble number with $a_n = 1$, we conclude

$$(n_0, \Delta n) = (q_{n-1}, q_{n-2} - 1). \quad (\text{B.31})$$

To put it more concretely, hereafter we restrict ourselves to the most important case of the golden angle in Eq. (B.10). The principal convergent p_n/q_n , $\Delta\alpha$ and $(n_0, \Delta n)$ are presented in Table B.3. In this simplest case, we have $p_n = F_n$ and $q_n = F_{n+2}$, where F_n is the Fibonacci number defined by the recurrence

$$\begin{aligned} F_0 &= 0, \\ F_1 &= 1, \\ F_n &= F_{n-1} + F_{n-2}. \quad (n > 1) \end{aligned}$$

(Table B.4.) The number of phyllotactic transition N_{PT} simply counts the number of p_n/q_n . Consequently, we obtain $N_{\text{PT}} = 2n + 1$ for

$$\frac{p_{2n}}{q_{2n}} < \alpha < \frac{p_{2n+1}}{q_{2n+1}} \quad (\text{B.32})$$

and

$$q_{2n+1} \leq n_c < q_{2n+2}. \quad (\text{B.33})$$

In terms of F_n , we obtain $N_{\text{PT}} = 2n + 1$ for $F_{2n+3} \leq n_c < F_{2n+4}$, and $\Delta\alpha = 1/(F_{2n+2}F_{2n+3})$. As a result, irrespective of whether n is even or odd, we obtain

$$N_{\text{PT}} = n \quad (\text{B.34})$$

for

$$F_{n+2} \leq n_c < F_{n+3}, \quad (\text{B.35})$$

and

$$\Delta\alpha = \frac{1}{F_{n+1}F_{n+2}}. \quad (\text{B.36})$$

Using a formula ([9])

$$F_n = \frac{1}{\sqrt{5}} (\tau^n - (-\tau)^{-n}) \simeq \frac{\tau^n}{\sqrt{5}}, \quad (\text{B.37})$$

we may regard $n_c \simeq \tau^{N_{\text{PT}}+2.5}/\sqrt{5}$ by (B.35). Then, we get

$$N_{\text{PT}} = \log(\sqrt{5}n_c)/\log\tau - 2.5, \quad (\text{B.38})$$

and

$$\Delta\alpha = (\tau/n_c)^2. \quad (\text{B.39})$$

Thus N_{PT}/n_c and $\Delta\alpha$ vanish in the limit $n_c \rightarrow \infty$. The logarithmic dependence in Eq. (B.38) for the irrational number $\alpha = \tau^{-2}$ is contrasted with a linear dependence $N_{\text{PT}} \simeq n_c/n$ for a rational number $\alpha = 1/n$ (Fig. 12). These results are used to guess a growth index n_c inversely. To achieve accuracy of $\Delta\alpha = 0.02$ (i.e., $\alpha = 0.38 \pm 0.01$), we need $n_c \simeq 11$ according to Eq. (B.39). To obtain a parastichy pair $(F_{10}, F_{11}) = (55, 89)$ of a sunflower head, we have to attain $\Delta\alpha = \frac{1}{F_{10}F_{11}} = 1/4895$, for which we need $n_c \simeq 113$. Indeed this lies between $F_{11} \leq n_c < F_{12}$.

Appendix C. Deviation from Fraction

To generalize the discussion in Sec. 4, let us consider a minimum of $v(\alpha)$ around a mediant

$$\bar{\alpha} = \frac{m+p}{n+q} \quad (\text{C.1})$$

of reduced fractions m/n and p/q (Appendix A). As in Eq. (17), the minimal model for this purpose is given by

$$v(\alpha) = v_n V(n\alpha - m) + v_q V(q\alpha - p). \quad (\text{C.2})$$

Differentiating this with respect to α , and substituting Eq. (C.1), we obtain

$$v'(\bar{\alpha}) = nv_n V' \left(\frac{np - mq}{n+q} \right) + qv_q V' \left(\frac{qm - np}{n+q} \right). \quad (\text{C.3})$$

On physical grounds, it is natural to assume that $V(x)$ is an even function, $V(x) = V(-x)$. Then, because of $V'(x) = -V'(-x)$,

$$v'(\bar{\alpha}) = (qv_q - nv_n) V' \left(\frac{mq - np}{n+q} \right). \quad (\text{C.4})$$

By definition, $V(\alpha) = V'(\alpha) = 0$ for $\alpha > X$. Hence, we get $v'(\bar{\alpha}) = 0$ for $X < \bar{X}$, where $\bar{X} = |mq - np|/(n+q)$. Without loss of generality, we may assume

$$\frac{m}{n} < \frac{p}{q}. \quad (\text{C.5})$$

Table B.3: The main sequence with the limit divergence angle $\alpha = \tau^{-2}$.

n	1	2	3	4	5	6	7	8	9	10
$\frac{p_n}{q_n}$	$\frac{1}{2}$	$\frac{1}{3}$	$\frac{2}{5}$	$\frac{3}{8}$	$\frac{5}{13}$	$\frac{8}{21}$	$\frac{13}{34}$	$\frac{21}{55}$	$\frac{34}{89}$	$\frac{55}{144}$
n_0	1	2	3	5	8	13	21	34	55	89
Δn	0	0	1	2	4	7	12	20	33	54
$\Delta\alpha$	1	$\frac{1}{2}$	$\frac{1}{6}$	$\frac{1}{15}$	$\frac{1}{40}$	$\frac{1}{104}$	$\frac{1}{273}$	$\frac{1}{714}$	$\frac{1}{1870}$	$\frac{1}{4895}$
\bar{X}	$\frac{1}{2}$	$\frac{1}{3}$	$\frac{1}{5}$	$\frac{1}{8}$	$\frac{1}{13}$	$\frac{1}{21}$	$\frac{1}{34}$	$\frac{1}{55}$	$\frac{1}{89}$	$\frac{1}{144}$

Table B.4: Fibonacci sequence.

n	0	1	2	3	4	5	6	7	8	9	10	11	12
F_n	0	1	1	2	3	5	8	13	21	34	55	89	144

Using $mq - np = 1$ ([9]), we obtain

$$\bar{X} = \frac{1}{n+q} \quad (\text{C.6})$$

for $(m+p)/(n+q)$. The optimal width \bar{X} for a fraction p/q is given by $\bar{X} = 1/q$. For $X < \bar{X}$, the potential $v(\alpha)$ is nearly constant for

$$\frac{m}{n} + \frac{X}{n} < \alpha < \frac{p}{q} - \frac{X}{q}, \quad (\text{C.7})$$

the width of which is

$$\Delta\alpha_{\text{flat}} = \left(1 - \frac{X}{\bar{X}}\right) \Delta\alpha, \quad (\text{C.8})$$

where we used Eqs. (A.2) and (C.6). The optimal width $\bar{X} = 1/q_n$ for the main sequence is given in Table B.3.

Strictly speaking, the minimum is not at $\alpha = \bar{\alpha}$ in Eq. (C.1), but lies at $\alpha = \bar{\alpha} + \delta\alpha$ by which a small correction $\delta\alpha$ is defined. Let us find $\delta\alpha$ by the condition $v'(\bar{\alpha} + \delta\alpha) = 0$. In the lowest order in $\delta\alpha$, we have

$$v'(\bar{\alpha} + \delta\alpha) = (qv_q - nv_n)V'(\bar{X}) + (n^2v_n + q^2v_q)\delta\alpha V''(\bar{X}). \quad (\text{C.9})$$

Hence we find

$$\delta\alpha = \frac{nv_n - qv_q}{n^2v_n + q^2v_q} \left(\frac{-V'(\bar{X})}{V''(\bar{X})} \right). \quad (\text{C.10})$$

By the assumption that $V(x)$ is localized with a half width X around $x = 0$, it is physically reasonable to suppose $V'(\bar{X}) < 0$ and $V''(\bar{X}) > 0$ at a tail of $V(x)$. Accordingly, the sign of $\delta\alpha$ is determined by the difference between the denominators of the parent fractions m/n and p/q . Under a weak condition that v_n decreases more rapidly than $1/n$, around a mediant $\bar{\alpha} = (m+p)/(n+q)$ between parent fractions m/n and p/q , a minimum of $v(\alpha)$ is slightly

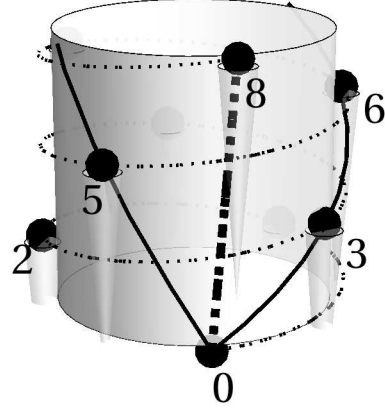


Figure C.21: A 'vascular leaf-trace primordium' of an 8-parastichy (dashed line) for $\alpha = 3/8 + \delta\alpha$ ($\delta\alpha = 0.003, n_c = 6$) is shown along with a parastichy pair (3,5) (solid lines). The sign of $\delta\alpha$ coincides with the sign of $2/5 - 3/8 > 0$, thereby the divergence angle α is slightly shifted from the PF $3/8$ toward a limit $\alpha = 0.382$.

shifted from $\alpha = \bar{\alpha}$ to the side of m/n or p/q with a larger denominator. This is consistent with Levitov's maximal denominator principle on a Farey tree ([14]). For instance, the position of the minimum in Fig. 16 is slightly shifted from $3/8$ to the side of $2/5$ (instead of $1/3$). The effect of $\delta\alpha$ is neglected in Sec. 3. It is surely negligible mostly as confirmed explicitly. Still there are cases where the deviation $\delta\alpha$ has discernible effects. First of all, non-zero $\delta\alpha$ deforms an 'orthostichy' $\alpha = (m+p)/(n+q)$ into a parastichy (Appendix A). According to the above theorem, the sign of $\delta\alpha = \alpha - (m+p)/(n+q)$ is given by the sign of $m/n - (m+p)/(n+q)$ ($n > q$) (Fig. C.21). The deviation from a fraction $\delta\alpha$ tends toward a limit divergence angle (Sec. 3.5).

Dynamical models aim to derive $\alpha = 1/\tau^2$ determin-

istically ([1, 20, 14, 6]). Their results are consistent with each other. The original idea of the dynamical mechanism can be traced back to [26] and [22]. Most of them are based on a *geometric* assumption that the interaction $V(|r_m - r_n|)$ depends only on the distance $|r_m - r_n|$ between the two points n and m . Generally, in an anisotropic system like plants, the assumption does not hold true. In short, a leaf is not a sphere on a cylinder surface (Fig. 1). If we had adopted this strong assumption, we would have failed to reproduce PFs. This is because $\delta\alpha$ enforced by the assumption is relatively large and not negligible. To compare with our model, however, it must be remembered that dynamical models mostly follow a long tradition of research focused on shoot apices. Unlike ours, they are not aimed at PFs of mature leaves.

Finally, as a possible generalization, let us mention a dynamical variant of our model. In the dynamical model, any slight deviation $\delta\alpha$ can be effectively important to determine a dynamical path of α . In the main text, we assumed that α_0 is a preset constant independent of n_c . In contrast, one may consider a model in which α_0 is variable such that $\alpha = \alpha_{\min}$ to minimize $v(\alpha)$ at a growth step n_c determines the initial value α_0 of the next step $n_c + 1$, i.e.,

$$\alpha_0(n_c + 1) = \alpha_{\min}(n_c), \quad (\text{C.11})$$

or let α_0 evolve continuously or adaptively along a branch in the tree of Fig. 4. To begin with, the initial condition must be set for $\alpha_0(1)$. To avoid confusion, α_0 of this model should rather be written as α . Consider what happens when a local maximum begins to appear around a minimum at $\alpha = \alpha_{\min}$, when n_c reaches $n_0 + \Delta n$ for α_{\min} . The maximum occurs just at a rational number near but not at α_{\min} . As discussed above, α_{\min} is shifted by a finite amount $\delta\alpha$ from the position of the maximum. Therefore, the sign of $\delta\alpha$ uniquely determines the next minimum to be chosen. Between two newborn daughter fractions, the one with a larger denominator is always chosen (a daughter fraction with a larger denominator lies on the same side of a parent fraction with a larger denominator). Thus, we obtain $\alpha \gtrsim 1/3$ at $n_c = 2$, then $\alpha \lesssim 2/5$ at $n_c = 3$, and $\alpha \gtrsim 3/8$ at $n_c = 5$, then $\alpha \lesssim 5/13$ at $n_c = 8$, and so forth. By following the main branch of Fig. 4, we reach $\alpha = 1/\tau^2$ finally in the limit $n_c \rightarrow \infty$. The bifurcation rule of this dynamical mechanism accords with (H) in Sec. 3.3. Nonetheless, the causal relationship between PFs and the golden angle is reversed here. In the dynamical mechanism, the golden angle is the *effect*, or the end result $\alpha(\infty)$ to be obtained generally. In the static mechanism, it is the *cause* $\alpha(0)$ to be selected specifically.